PHYSICAL REVIEW A **87**, 041802(R) (2013)

Time-domain mapping of nonlinear pulse propagation in photonic-crystal slow-light waveguides

F. Raineri,[1,2] T. J. Karle,[3] V. Roppo,[1] P. Monnier,[1] and R. Raj[1,*]

[1]*Laboratoire de Photonique et de Nanostructures, Route de Nozay, Marcoussis 91460, France*

[2]*Université Paris Diderot, Paris 75205 Cedex 13, France*

[3]*School of Physics, University of Melbourne, Victoria 3010, Australia*

(Received 8 January 2013; published 12 April 2013)

We perform an experimental time-domain mapping of nonlinear pulse propagation through a two-dimensional photonic-crystal waveguide. Our optical gating method allows for the complete reconstruction of the peculiar propagation behavior in this highly dispersive structure. Temporal soliton formation is accompanied by fast time-scale dynamics within the picosecond pulse regime. For high signal powers, the photonic waveguide band is modified, leading to an acceleration of the propagated pulse.

DOI: 10.1103/PhysRevA.87.041802 PACS number(s): 42.70.Qs, 42.79.Hp, 42.81.Dp

Two-dimensional photonic crystals (2D PhC) have been the subject of extensive studies in recent years due to their unique ability to control light propagation [1–3] thanks to the engineering of their dispersive properties. PhCs, providing, as well, strong field confinement in microscale semiconductor waveguides, can be considered an ideal platform for exploring nonlinear optical effects. They have already shown outstanding performance in terms of power efficiency and footprint in switches [4–6] and lasers [7].

Solitons have captured the attention of researchers in a wide variety of domains ranging from hydrodynamics to biology as well as plasma physics and nonlinear optics. In optics, the solitary wave evolves from the interplay of the group-velocity dispersion and the self-phase modulation due to the nonlinear change in the refractive index. For usual values of optical intensity and material nonlinearity, the space scale over which soliton propagation can be observed, spans from centimeters to meters [8].

In the particular case of 2D PhCs, GaInP line defect waveguides [Fig. 1(a)], the low group-velocity (v_g) regime leads to the formation of temporal solitons in only a few millimeters of propagation distance [9]. Close to the photonic mode edge of this PhC waveguide, the nonlinearities are readily accessed as they scale with the group index of refraction, which varies from 4 to 20 in a 40-nm wavelength span [see, for example, Fig. 1(b)]. Thus, it is easy to understand why this kind of structure provides an interesting and unique tool for the investigation of the behavior of temporal solitons with spectral bandwidths on the order of nanometers.

In order to exploit the advantages provided by the low-v_g regime, precise characterization and management of the group velocity is essential. Experimentally, the time-domain mapping of pulses propagating through the waveguide is conventionally characterized using pulse autocorrelation techniques [10]. However, this method prevents the investigation of the complex internal structure of the pulse, which can be modified by subtle effects, such as the nonlinear dispersion and transit delay with respect to the linear propagation.

This lack of knowledge in the precise temporal behavior of the propagating pulses, on one side, can affect the practical engineering with errors in the control of the dispersion of the device and, on the other side, will shade the emersion of fundamental physics in the propagation characteristics.

For these reasons, in this Rapid Communication, we carried out a direct reconstruction of the time-domain dynamics of temporal solitons using a parametric amplification optical gating method. We report the result of the cross correlation with 90-fs reference pulses which allows us to retrieve the precise dynamic behavior of the pulse after its nonlinear propagation through the waveguide.

Our detailed experimental analysis is applicable and desirable for *any* situation of pulse propagation. However, it is in the soliton formation environment where it becomes essential as the huge group-velocity dispersion in PhC waveguides combined with Kerr nonlinearity induces ultrafast dynamics in the electromagnetic field even for picosecond pulses with energies of only 10 pJ.

Our PhC sample is an $L = 1.3$-mm-long W1 waveguide formed by one line of missing holes along the ΓK direction in a hexagonal lattice of air holes drilled in a GaInP slab membrane [9]. The schematic of the experimental setup is shown in Fig. 2. An OPA provides 90-fs pulses at wavelengths around 1.55 μm. Before being injected into the sample, the pulses pass through a Dazzler [11] acousto-optical pulse shaper (D), which is used to obtain the desired pulse shape, i.e., a 2.2-ps-long Gaussian pulse.

The sample is mounted on a nanopositioning stage, and optical pulses are end-fire coupled via aspheric lenses. After propagating through the PhC waveguide, the transmitted signal is split between a SP and the nonlinear optical gating setup. To gate the dispersed signal outputting the PhC waveguide, we recombine it with powerful 800-nm 90-fs pulses in a β-barium borate (BBO) crystal. The nonlinear interaction between the two pulses amplifies the signal from the waveguide in the range of 1490–1565 nm. The angle θ of the BBO crystal is varied in order to phase match the interaction. The 800-nm pump pulses are frequency doubled within the crystal to produce a blue pump at 400 nm which enables the parametric amplification of the infrared signal and the generation of a complementary green signal at 540 nm. This is preferred to the up-conversion gating technique [12,13] as it provides higher levels of signals.

A few additional steps are required to eliminate the background noise. First, the green photons are efficiently

*Corresponding author: rama.raj@lpn.cnrs.fr

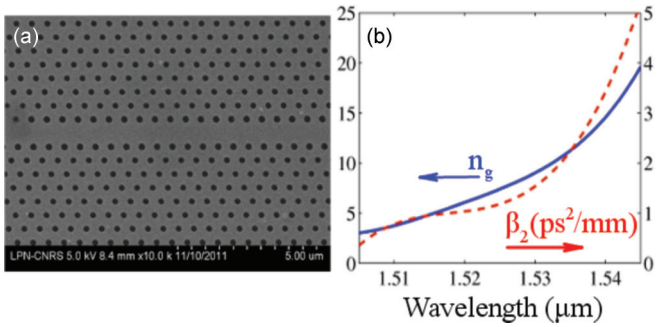

FIG. 1. (Color online) (a) SEM image of the sample. (b) Group index and group-velocity dispersion dependences on wavelength and fit of experimental values.

detected using a GaP photomultiplier detector. The intense red 800-nm pump pulses are suppressed with a long-pass filter (F2 in Fig. 2). The green signal is detected in a background-free configuration, avoiding the blue light arising from the frequency doubling of the pump by using a 10° angle between the signal to be measured and the pump. Residual stray light is eliminated using a bandpass filter at 540 nm (F1 in Fig. 2). Finally, the more insidious noise due to the parametric *fluorescence* induced by the pump at 540 nm alone of 550 nm is eliminated electronically through synchronous detection.

The temporal mapping is carried out by optically delaying the 800-nm pump pulse with respect to the signal and recording the parametrically amplified signal as a function of the delay. It is, thus, possible to map the temporal response of the pulses transmitted by the waveguide with a resolution of 90 fs.

Prior to the investigation of the nonlinear optical response, we performed a time-of-flight characterization of the linear pulse propagation through these waveguides using our parametric amplifier gating method. This directly measures the linear time delay Δt of the pulses as a function of wavelength. This characterizes the linear dispersion of the

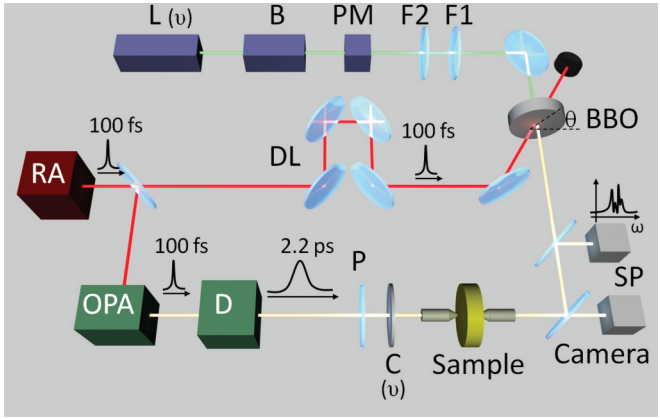

FIG. 2. (Color online) Ultrafast measurement setup. Ti:sapphire regenerative amplifier (RA) providing 90-fs 810-nm pulses to an optical parametric amplifier (OPA), which, in turn, supplies a 1550-nm idler to the D: Dazzler pulse shaper; other optics, P: polarizer; C: chopper; DL: delay line; SP: spectrometer; F1: bandpass filter; F2: long-pass filter B18; PM: photomultiplier; B: boxcar; and L: lock-in amplifier.

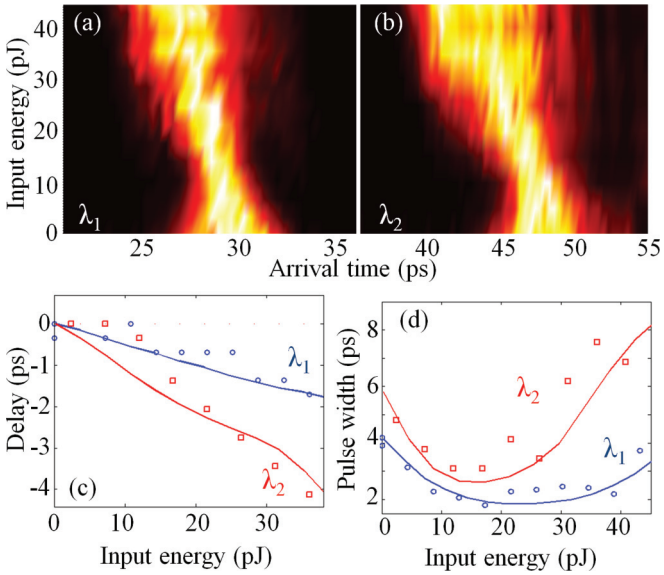

FIG. 3. (Color online) Pulse reconstruction for different input powers. Experimental results for (a) $\lambda_1 = 1525$ nm and (b) $\lambda_2 = 1535$ nm. Each measurement is normalized to the peak value. (c) Delay with respect to the linear arrival time and (d) pulse widths as a function of the input power: points: experimental results and solid line: calculations.

waveguide, directly yielding the group index curve $n_g = c\,\Delta t/L$ [Fig. 1(b)]. The figure shows the dramatic increase in n_g as the wavelengths approach the band edge of the PhC.

For a wavelength of $\lambda = 1525$ nm, the linear dispersion length and the effective length are defined, respectively, by $L_d = \tau^2/\beta_2$ and $L_{\text{eff}} = 1/\alpha_1$ where τ is the pulse duration, β_2 is the second-order term of the group-velocity dispersion [Fig. 1(b)], and α_1 is the linear losses (absorption, scattering,...). In our system, L_d and L_{eff} are both on the order of the length of the waveguide, i.e., a few millimeters.

We then measured the temporal evolution of the 2.2-ps pulses transmitted through the waveguide as a function of the incident pulse energy for different wavelengths. As an example, in Figs. 3(a) and 3(b), the evolution of the pulse as a function of the input pulse energy for $\lambda_1 = 1525$ and $\lambda_2 = 1535$ nm is reported. Figure 3(c) shows the delay with respect to the low energy and linear arrival time, and Fig. 3(d) shows the pulse width (FWHM), both plotted as a function of the input pulse energy.

In the low-intensity regime (<1 pJ), the 2.2-ps pulse broadens during the propagation due to the linear dispersion and chirp, reaching widths of 4.2 or 5.9 ps at the end of the waveguide for λ_1 and λ_2, respectively.

The increase in the pulse energy coupled into the sample accesses the nonlinearity of the GaInP material. In the range of 1–15 pJ, the pulse width narrows for both wavelengths clearly showing the formation of temporal solitons. From Fig. 3(d), we can see that, for an input energy of 20 pJ at $\lambda_1 = 1525$ nm, a 2.2-ps pulse is compressed to form a soliton that propagates with a FWHM of ~2 ps.

In the soliton theory, it is handy to introduce the soliton number $N_s = L_d/L_{nl}$, given by the ratio between the dispersion length and the nonlinear lengths $L_{nl} = 1/\gamma P$, where

γ is the third-order nonlinearity and P is the pulse power. Values on the order of $N_s = 1$ indicate that the dispersion and self-modulation effects are nominally compensated. N_s monotonically increases with the coupled energy, and values greater than $N_s = 1$ indicate the potential formation of higher-order solitons with multifold periodical temporal evolution of the pulse envelope.

The calculated soliton number for an energy of 20 pJ is $N_s = 2.5$. This means that, in an ideal situation, we should already be in the presence of a second- or third-order soliton. However, in our case, the strong influence of the three-photon absorption (ThPA) of the material [9] sensibly reduces the available power during the propagation and, thus, the nominal N_s with the consequence that we can observe a simpler first-order soliton.

More importantly, in Fig. 3(c), we can note that the arrival time of the pulse is significantly advanced with respect to that for lower input pulse energy. The pulses arrive up to 4 ps earlier than at lower pulse energies. This pulse acceleration could not be detected with conventional autocorrelation methods.

In the high-energy regime (>20 pJ), other nonlinear effects start to take part in the propagation dynamics. We observe a constant advance of the pulse, reaching 0.05–0.1 ps/pJ with respect to the linear low-energy situation for λ_1 and λ_2, respectively. This temporal advance is on the order of the pulse width. Although we would expect the pulses to continue to narrow for increasing energy (remembering that $N_s \gg 1$), we, instead, record a counterintuitive broadening of the pulse width that reaches values >5 ps for energies on the order of 45 pJ [Fig. 3(d)].

Notice that the actual energy inside the sample is lower due to imperfect coupling. We estimate 4-dB energy insertion losses at the input and output for a total linear transmittance of 11%.

To explain both the unexpected acceleration and the broadening at high pulse energies, we perform a numerical analysis of the nonlinear interaction. The transversal confinement of the field allows us to decouple the dynamics and to focus our attention only in the longitudinal direction. The input field has the shape,

$$E(z=0,T) = E_0 \exp[-(1+iC)T^2/2\tau^2], \tag{1}$$

where E_0 is the initial peak value and C is the initial linear chirp, estimated as $C = 0.8$. We work in a retarded reference frame with $T = t - z/v_g$. We then assume that the propagation is well described by a time-domain one-dimensional nonlinear Schrödinger equation,

$$\frac{\partial E}{\partial z} = -i\frac{\beta_2}{2}\frac{\partial^2 E}{\partial T^2} - \frac{\alpha_1}{2}E + \left(i\gamma_{\text{eff}} + \gamma_1\frac{\partial}{\partial T}\right)|E|^2 - i\delta_{\text{eff}}|E|^4 E - \frac{\alpha_{3\text{eff}}}{2}|E|'^4 E, \tag{2}$$

where

$$\alpha_{3\text{eff}} = \frac{\alpha_3 n_g^2}{A_{5\text{eff}}^2}, \quad \gamma_{\text{eff}} = \frac{n_2\omega_0}{cA_{\text{eff}}}\left(\frac{n_g}{n_{\text{bulk}}}\right)^2,$$

and

$$\delta_{\text{eff}} = \frac{n_4\omega_0}{cA_{\text{eff}}^2}\left(\frac{n_g}{n_{\text{bulk}}}\right)^2$$

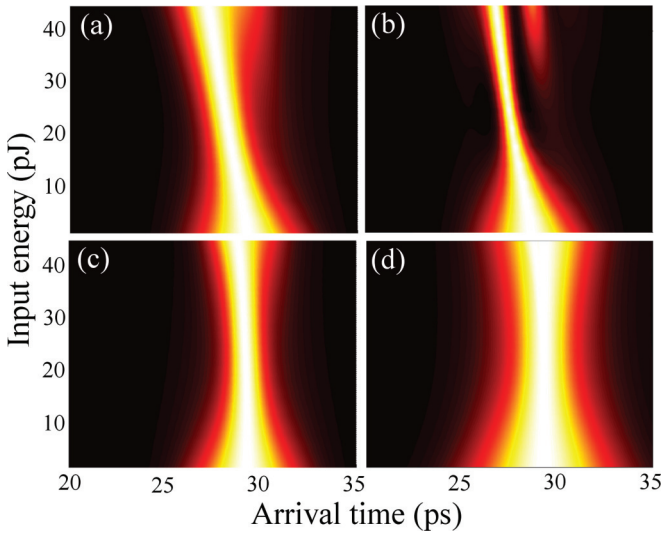

FIG. 4. (Color online) Results of the calculation for $\lambda_1 = 1525$ nm. (a) Pulse reconstruction for different input powers. (b) Case with $n_4 = 0$. (c) Case with $\gamma_1 = 0$. (d) Results after the autocorrelation.

are the scaled values of the nonlinear coefficients describing the ThPA, third- [9], and quintic-order [14–16] nonlinearities, respectively. $n_{\text{bulk}} = 3.12$ is the index of refraction of InGaP, $\omega_0 = 2\pi c/\lambda$, c is the speed of the light in the vacuum, A_{eff} and $A_{5\text{eff}}$ are effective areas given by the transverse localization of the field in waveguides [9].

The wavelength dependence of the third-order nonlinear coefficient has been taken into account by introducing the first-order Taylor expansion in the frequency domain around ω_0,

$$\gamma(\omega) = \gamma_{\text{eff}}(\omega_0) + (\omega-\omega_0)\frac{\partial\gamma_{\text{eff}}}{\partial\omega}\bigg|_{\omega_0} = \gamma_{\text{eff}}(\omega_0) + \gamma_1(\omega-\omega_0). \tag{3}$$

In Eq. (2), we omitted the terms for the effects of third-order dispersion ($\beta_3 = 0.053$ ps^3 mm^{-1}) and free carriers ($N_c \sim 10^{15}$ cm^{-3} at maximum) having verified that they could be neglected in our operating regime. The equation is solved via a standard fast-Fourier-transform-based split-step beam propagation method [8], and the results are depicted in Figs. 3(c) and 3(d) (solid line) and Fig. 4. In particular, in Fig. 4(a), the pulse reconstruction is plotted for different input energies for $\lambda_1 = 1525$ nm and can be compared to Fig. 3(a). In Figs. 3(c) and 3(d), we plot the calculated pulse delay and widths. The agreement with the experimental results is evident.

We have introduced two terms into Eq. (1) to explicitly model our experimental results. First, a δ_{eff} term, which depends on n_4 accounts, at the first order, for the saturation of the Kerr effect of the material at high intensities [12]. Including the quintic order, the nonlinear index can be written as

$$n = n_0 + n_2 I - n_4 I^2. \tag{4}$$

The saturation point is nominally reached at the intensity given by $I_{\text{sat}} = n_2/2n_4$ [14]. For $\lambda_1 = 1525$ nm, considering 20 pJ as the saturation point, (the point where we obtain the maximum

nonlinear index), we can estimate $n_4 \sim 1.0 \times 10^{-31}$ m^4/W^2. Our theory, including n_4, accurately reproduces the narrowing to a minimum of 2 or 2.9 ps for λ_1 and λ_2, respectively, and the subsequent broadening for higher energies. In Fig. 4(b), we show the results in the case where we set $n_4 = 0$. The pulse preserves the acceleration, but it continues to be compressed as predicted by the pure-n_2 soliton theory. The maximum compression reaches values of ~0.5-ps FWHM, and we can observe the presence of high-order solitons at high energies. Even if the dynamics involved are very rich, we strongly believe that the observed behavior can be explained excluding effects other than high-order Kerr effects. On the other hand, we do not exclude that, for higher-energy regimes, similar effects can also stem from higher than quintic-order contributions to the nonlinear index.

Second, the $|E|^2$ term that depends on γ_1 in Eq. (1) is responsible for the acceleration of the propagating pulse. Due to the strong dispersion of γ_{eff}, it is important to include the effect of the first order of the Taylor expansion around ω_0. The analytical expression of γ_1 is given by

$$\frac{\gamma_1}{\gamma_{\text{eff}}} = \left(\frac{1}{\omega_0} + \frac{2}{n_g}\frac{\partial n_g}{\partial \omega} - \frac{1}{A_{\text{eff}}}\frac{\partial A_{\text{eff}}}{\partial \omega} + \frac{1}{n_2}\frac{\partial n_2}{\partial \omega} \right). \quad (5)$$

In the case of *bulk* material, with a negligible dispersion of n_2, Eq. (4) reduces to $\gamma_1/\gamma = 1/\omega_0$ (on the order of a few femtoseconds) [17], and it is easy to recognize the correspondent term in Eq. (2) as the so-called *shock term*. This term has been deeply studied for *ultrashort* pulses (~10-fs long) [8,17,18] where it produces a shift in the peak of the propagating pulse. In the other regimes, it is generally negligible. However, in our particular case, the full expression must be considered due to the strong variation in the group index and the effective area. To fit the experimental results in this Rapid Communication, we have taken $\gamma_1/\gamma_{\text{eff}} = 0.20$ and 0.24 ps for λ_1 and λ_2, respectively. This is in agreement with the values given in Ref. [9] where, with a mixture of three-dimensional FDTD calculations and material characterizations, it has been estimated that, for these particular GaInP line defect waveguides, the value of γ_1 can vary in the range of $\gamma_1/\gamma_{\text{eff}} = [0.1 - 0.4]$ ps.

In Fig. 4(c), we show the results of the calculation as in Fig. 4(a) but setting $\gamma_1 = 0$. The pulse preserves the narrowing and broadening effects due to the interplay of n_2 and n_4, but its arrival time at the end of the waveguide is constant. Therefore, it is clear that the acceleration is due to the enhancement of the shock term in the picosecond regime.

Finally, in Fig. 4(d), we plot the results after we performed an intensity *autocorrelation* as we expect from classical autocorrelation measurements. It is easy to see that the acceleration of the pulse is not detectable. This is a clear example on how our gating method is able to unveil fundamental dynamics, otherwise, experimentally inaccessible.

In conclusion, we have experimentally explored the effects of dispersion and nonlinearity on picosecond pulse propagation in a 2DPhC line-defect waveguide. In this Rapid Communication, an optical gating technique has been successfully applied to carry out an in-depth analysis of the temporal dynamics of soliton propagation. The signal mapped by the parametric amplification demonstrates the formation of solitons at specific wavelengths and input powers. This corresponds to the delicate balance between the group-velocity dispersion and the self-phase modulation for an input energy on the order of 20 pJ. At higher signal powers, the group velocity is strongly modified by higher-order nonlinear effects leading to an acceleration of the pulse.

Our time-domain analysis is crucial for PhC waveguides as the interplay between the large group-velocity dispersion and the low group-velocity/high-field confinement of the optical modes allows us to observe solitons for tens of picojoules of input power.

The harnessing of these characteristics, through controlled tailoring of the structure, will permit precise dispersion control, applicable to group delay lines, pulse shaping, and dispersion compensation devices at telecom wavelengths.

F.R., T.J.K., V.R., and R.R. have equally contributed to this work. The authors thank A. De Rossi, S. Combrié, and P. Colman for providing the sample and N. Forget and P. Tournois of FastLite for support with the Dazzler. They acknowledge the FP7 COPERNICUS European project for funding.

[1] T. Baba, Nat. Photonics **2**, 465 (2008).
[2] H. Gersen, T. J. Karle, R. J. P. Engelen, W. Bogaerts, J. P. Korterik, N. F. van Hulst, T. F. Krauss, and L. Kuipers, Phys. Rev. Lett. **94**, 073903 (2005).
[3] T. J. Karle, Y. J. Chai, C. N. Morgan, I. H. White, and T. F. Krauss, J. Lightwave Technol. **22**, 514 (2004).
[4] N. K. Nozaki, T. Tanabe, A. Shinya, S. Matsuo, T. Sato, H. Taniyama, and M. Notomi, Nat. Photonics **4**, 477 (2010).
[5] F. Raineri, C. Cojocaru, P. Monnier, A. Levenson, and R. Raj, Appl. Phys. Lett. **85**, 1880 (2004).
[6] C. Husko, A. DeRossi, S. Combrié, Q. V. Tran, F. Raineri, and C. W. Wong, Appl. Phys. Lett. **94**, 021111 (2009).
[7] Y. Halioua, T. J. Karle, F. Raineri, P. Monnier, I. Sagnes, G. Roelkens, D. Van Thourhout, and R. Raj, Appl. Phys. Lett. **95**, 201119 (2009).
[8] G. P. Agrawal, *Nonlinear Fiber Optics*, 4th ed. (Academic Press, San Diego, 2006).
[9] P. Colman, C. Husko, S. Combrié, I. Sagnes, C. W. Wong, and A. De Rossi, Nat. Photonics **4**, 862 (2010).
[10] T. Asano, K. Kiyota, D. Kumamoto, B.-S. Song, and S. Noda, Appl. Phys. Lett. **84**, 4690 (2004).
[11] http://www.fastlite.com.
[12] F. Raineri, A. M. Yacomotti, T. J. Karle, R. Hostein, R. Braive, A. Beveratos, A. Sagnes, and R. Raj, Opt. Express **17**, 3165 (2009).
[13] N. Bouché, C. Dupuy, C. Meriadec, K. Streubel, J. Landreau, L. Manin, and R. Raj, Appl. Phys. Lett. **73**, 2718 (1998).
[14] B. Borchers, C. Brée, S. Birkholz, A. Demircan, and G. Steinmeyer, Opt. Lett. **37**, 1541 (2012).

[15] As our results suggest, we assume that n_4 has the same scaling as γ_{eff} with the group index.

[16] A. Desyatnikov, A. Maimistov, and B. Malomed, Phys. Rev. E **61**, 3107 (2000).

[17] E. N. Tsoy and C. M. De Sterke, J. Opt. Soc. Am. B **23**, 2425 (2006).

[18] P. V. Mamyshev and S. V. Chernikov, Opt. Lett. **15**, 1076 (1990).